ES91R Spring 2020 Research Summary Report

Robert Jomar Malate
S.B. Mechanical Engineering
Harvard University
Cambrdige, MA, USA
robertjomarmalate@college.harvard.edu

***Abstract*—This paper aims to summarize my work performed in the Harvard Microrobotics Lab. In the first half of the semester, I focused on the design, manufacturing, and experimentation of new components for the Harvard Robobee. In addition, I also worked on the research and design of a novel vertical hopping microrobot and a 2 degree-of-freedom (DOF) joint. During the second half of the semester, using finite-element analysis (FEA), I analyzed optimal wing designs of the Robobee wing, keeping the wing area constant while parametrizing the spar distance and spar angles of the wing frame.**

I. Introduction

Throughout the Spring 2020 semester, I was working in the Harvard Microrobotics Lab under the mentorship of Avik De (James S. McDonnell Foundation Postdoctoral Fellow). At this time, I worked on various aspects of the Harvard Robobee project, such as testing new wing designs to assisting the development of an optimization tool, and the creation of new robot system and parts design.

Interestingly, because of the type of work performed and the COVID-19 situation, this paper is organized by talking about the work done during the first and second halves of the Spring 2020 semester. In addition, the themes of breadth and depth are expressed during these time periods, which will be made clear by the type of work done during those respective time periods.

II. Design and Manufacturing of Micro-scale Flapping and Hopping Robots

The work accomplished in the 1st-half of the semester can be separated into three subprojects: optimization tool of the Robobee, designing a vertical hopping microrobot, specifically, a passive flexure and a 2 DOF joint. During this period of the project, the principles of design, manufacturing, and experimentation took place, albeit at different degrees for each project. This section describes the work that has been done for each section and to the extent the three principles occurred.

A. Optimization Tool for Harvard Robobee

A large portion of this time period was dedicated to the design and experimentation of the wing and transmission of the Robobee. This was to help with the development of an optimization tool that given desired output kinematics and interaction forces outputs an optimal design for various parts of the robot. We discuss the work that has been done.

1) Wings: A lot of time was spent on designing and experimenting with new wing designs. Using computer-aided design (CAD) software, specifically AutoCAD, I began the process by redesigning old wing designs, which acted as a reference model. Various aspects of the wings were modified and treated as parameters, among these are the following: wing area, aspect ratio, spar length, and chord length. Refer to Table 1 for some examples of the new dimensions.

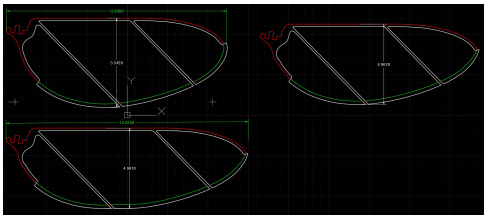

Fig. 1. Screenshot of some of the wings that were designed for the project.

The next part of the process was the manufacturing. Because of the scale of the parts of the Robobee, understanding the manufacturing methodology of smart composite microstructures (SCM) [1] was key. Using the DPSS laser, I learned and eventually assisted with the manufacturing of the wings. Essentially, for SCMs, each part is broken down into horizontal layers, with each layer having a different material. Each layer is then combined by heat and or pressure treatment, the final result being the fully assembled part.

Once the wings have been manufactured, we then began the experimentation. For all of the wings, we performed a static flapping tests. Here, a wing is attached to a Robobee frame to a hinge. The whole frame is then held in place and put in front of a high speed camera. With a MATLAB script sending voltage signals based on desired flapping frequencies, a recording is taken of the wing flapping. The video is then post processed and analyzed. For analysis, using ImageJ, I measured the stroke angle that each wing produces (refer to Fig. 3).

2) Transmission: In addition to the wing, I spent some time looking into the design of the transmission. This part transfers the force from the actuator to the flapping of the wing. Using the reference image for the transmission (Fig. 5), I experimented with different characteristic transmission lengths (L_1, L_2, L_{1o}, L_{2o}) by using a Mathematica script that Avik provided (refer to Fig. 6).

TABLE I
ORIGINAL AND MODIFIED WING DIMENSIONS

Wing Version	Wing Area (mm^2)	Aspect Ratio	Spar Length (mm)	Chord Length (mm)
Original	54.4	2.135	11.69	5.475
Wing 1	53.3518	2.66	13.27	4.988
Wing 2	46.6629	2.385	11.8981	4.988

*Table that showcases a few of the modified wings' dimensions with reference to original wing.

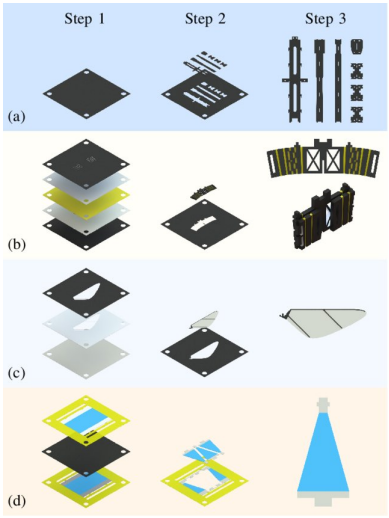

Fig. 2. Image of fabrication process for the various Robobe parts. Image obtained from [2]

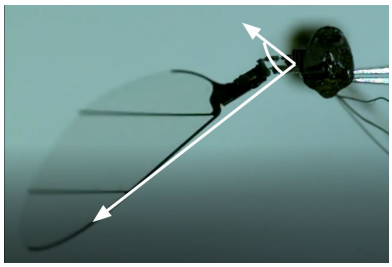

Fig. 3. Screenshot of stroke angle measurement.

At the time of the project, I did not have the chance to manufacture the transmissions and measure their performances.

B. Vertical Hopping Microrobot

1) 1 DOF Joint: After work on the optimization tool was completed, I began work on designing a vertical hopping robot. I was tasked to design the passive flexture in the "knee" joint. Inspired by the castellated joints in [3], I came up with the following joint designs presented in Fig. 7.

These joints enabled 1-DOF rotational motion while minimizing torsion. In addition, it exhibits spring-like behavior, which would be taken advantage of. The transmission would cause the joint to bend, storing energy. Once released, the stored energy would cause the joint to return to it's equilibrium position.

Fig. 4. Frame captured from the static flapping test. Stroke angle measurements are then taken from the videos.

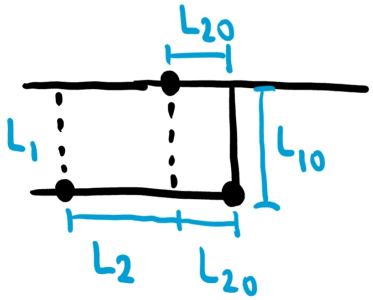

Fig. 5. Schematic for the dimensions of the transmission.

2) 2 DOF Joint: In addition to the "knee" joint, I also worked on designing a 2 DOF joint. It would be a passive joint that would be attached to a transmission. In addition to researching current designs ([4]) and drafting new ones with Avik (refer to Fig. 8 and Fig. 9), I also was trained on how to use to paper-laminate laser cutting, which is a method that tests SCM designs by building paper models.

III. WING DESIGN FINITE ELEMENT ANALYSIS

Due to the COVID-19 situation, the original research plan got disrupted; labs were shutdown and a large majority of the undergraduates required to moveout, myself included. Without access to the labs, it was impossible to manufacture and run experiments with new designs for the previous projects. To work around this, in conjunction with my Computational Structural and Solid Mechanics course (ENG-128/228), using ABAQUS, I proposed conducting a finite-element analysis (FEA) on the designs of the Robobee wing. Unfortunately, due to various technical errors, valid results were not able to be obtained. Nonetheless, this section aims to describe the processes that was undertaken in order to conduct the analysis and describe the issues encountered.

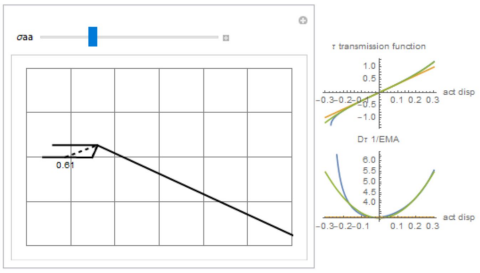

Fig. 6. Mathematica script that was used to analyze potential transmission designs. One optimization goal was to make the output match the green parabolic curve.

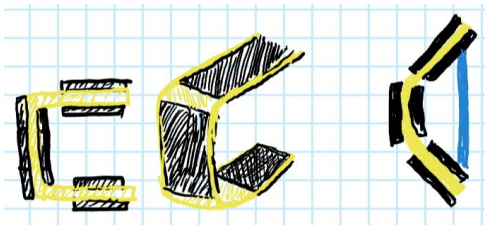

Fig. 7. Sketches of designs for the knee-joint. Due to the stiffness of the Kapton, it exhibits spring-like behavior which could be taken advantage of.

A. Goals, Parameters, and Constraints

Due to the complex nature of the Robobee wing and time constraints, we needed to define attainable goals yet while yielding valuable results. To accomplish this, we wanted to fulfill two objectives:

(I) Deflections on the spar need to be minimized. This would ensure that the wing is structurally stable and won't have fatigue issues [5].

(II) Moment of inertia around the z-axis needs to be minimized [6]. Referring to Fig. 10 for reference, reducing this inertia will enable the wing to operate more efficiently.

Looking at the two requirements, attaining an optimal balance is challenging. For instance, we can easily increase the amount of carbon fiber used in the wing frame, but that would in turn increase I_{zz} [6].

To find the optimal design that balances these two and setting the appropriate scope, we hold the wing area constant at A_{wing} = $54.4\,\mathrm{mm}^2$ while varying the following two parameters: (A) spar distance and (B) spar angles. Refer to Fig. 11 for a visual guide.

B. Model and Analysis Setup

To ensure that model is as close to the experimental configuration, we carefully setup the various ABAQUS parameters [8]. This section describes the setup.

1) Geometry: A couple of simplifications were made to the AutoCAD sketches. First, it was broken down into two parts, wing frame and wing membrane. Due to the complexity of the wing sketch geometry, we generated multiple wing frames sketches, each with different values for the parameters. For

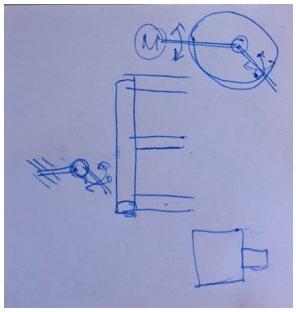

Fig. 8. Draft sketch of 2 DOF joint design proposed by Avik. This gave me the starting point for working on this aspect of the project.

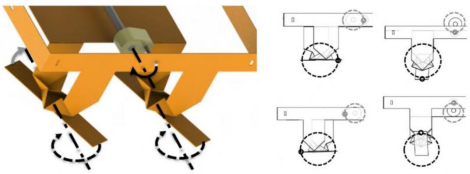

Fig. 9. Robot model that provides some guidance for the 2 DOF joint design. Obtained from [4]

the wing spar distance, we ranged it between about $5\,\mathrm{mm}$ to $9\,\mathrm{mm}$. The spar angle ranged between 35 to 60 degrees (refer to Fig. 11). These were all exported as .dxf files.

In addition, the curves at various points on the wing were angled. This was done in order to ensure that there were no oddly-shaped elements in the mesh. Refer to Fig. 12 for the points that were angled.

2) Materials: The original wing is composed of three layers: the frame, adhesive, and a membrane. Ignoring the adhesive, the materials for the two layers are carbon fiber and Mylar, respectively. For both materials, we assumed linear elastic behavior. Basing off the material specification sheet for Mylar [9], the values are $E = 3.447\,\mathrm{GPa}$ (Young's Modulus) and $\nu = 0.38$.

For the carbon fiber, the orientation needed to be taken into account. The carbon fiber that was used is YSH-50 (0-45-0). Based on this information and the specification sheet [10], we obtain the folllowing parameters that were inputted into ABAQUS:

- E_1 (Young's Modulus, 0 deg) = $310\,\mathrm{GPa}$
- E_2 (Young's Modulus, 90 deg) = $3.8\,\mathrm{GPa}$
- ν_{12} (In-plane Poisson Ratio, 90 deg) = 0.2
- G_{12} (In-plane Shear Modulus) = $4.8\,\mathrm{GPa}$
- G_{13} (Transverse Shear Modulus) = $245\,\mathrm{GPa}$
- G_{23} (Transverse Shear Modulus) = $245\,\mathrm{GPa}$

There was no specification given explicitly for G_{23}, but we assumed that G_{13} = G_{23}.

3) Boundary Conditions: Since the wings were attached to a hinge mechanism that was passively rotating, all translational and rotational degrees of freedom were constrained (U1 = U2 = U3 = UR1 = UR2 = UR3 = 0, written in ABAQUS convention). Although the hinge does allow free rotation, for the static and quasi-static analysis, the hinge is held in place.

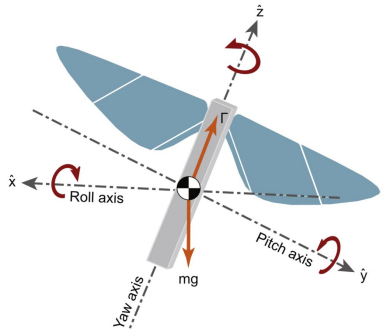

Fig. 10. Diagram that showcases the coordinate axes of the Robobee. Image obtained from Chirarattananon et al paper [7].

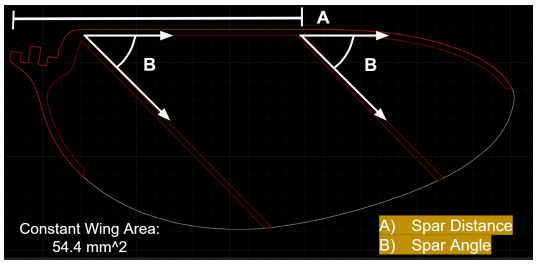

Fig. 11. Visual aid that showcases the parameters and constraints on the wing. Note that the wing frame (red) will be varied in the analysis. Spar distance (A) is the distance of the rightmost spar from the leftmost point on wing attachment. Spar angle (B) is the angle of the spars relative to the top edge of the wing frame. Wing area is constant (A_{wing} = 54.4 mm^2).

4) Loading: The drag force from the air is the largest force that the wing experiences during flapping. Although this is caused by fluid dynamic effects, because ABAQUS's CFD solver doesn't perform well and that we are interested in the wing behavior from a structural point of view, we treated the drag force as a pressure acting perpendicular to the surface of the wing. Since we are interested in the maximum deflection for each wing frame design, we needed to determine the maximum drag pressure that the wing experiences. The following equation modified from Whitney and Wood's paper [11] calculates the drag force on the wing. Note that the only modification was that the original equation was pertaining to lift (F_L and C_L). However, these can be changed to calculate for drag by using C_D instead.

$$F_D = \frac{1}{2}\rho\omega_h^2 C_D(\alpha)\bar{c}R^3\hat{F} \tag{1}$$

Assuming worse case angle of attack (α = 0) and applying the relevant parameters, we can determine the worse-case drag force experienced by the wing. Dividing this by the wing area, we get that P_{wing} = 128 Pa. The calculator and values used can be provided upon request.

5) Meshing: A crucial part of FEA, we selected the appropriate mesh configuration for the model. Although different mesh elements were tried, ultimately what was used are linear, tetrahedral elements (S3) for the wing frame, and linear, tetrahedral membrane elements (M3D3) for the wing membrane. Refer to Fig. 14 for a picture of the mesh.

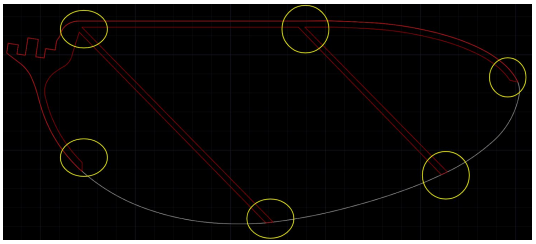

Fig. 12. Diagram that showcases the parts of the wing that were angled, indicated by yellow circles.

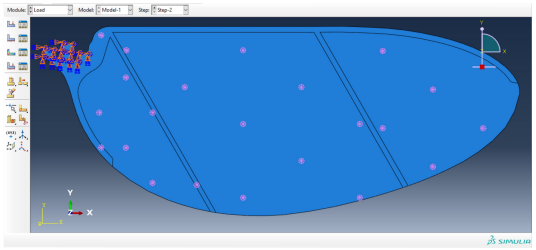

Fig. 13. Screenshot of boundary conditions and loads applied to the ABAQUS wing model.

The choice of using linear tetrahedral elements as driven by the failure of the experimental process. Originally, we were using quad-dominated elements, but due to the computational time increase and constant errors being raised, we decided switching over to tetrahedral elements would help us debug the issue. Although quadrilateral elements provide better accuracy, the teaching fellows of the course pointed out that linear elements would be satisfactory and would reduce computation time.

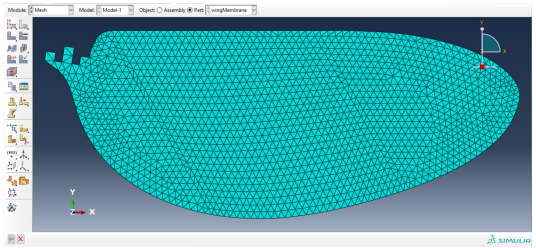

Fig. 14. Screenshot of the model mesh for the FEA. Linear tetrahedral elements were used for the whole model. The wing frame used shell elements (S4/S3) while the membrane used membrane elements (M3D3/M4D4).

C. Experimentation and Results

Using this setup, we then started conducting the analysis, with small changes to the steps made depending on the type of analysis performed. As was mentioned earlier, no usable results were obtained due to technical errors.

1) Static Analysis: Because we were interested in the structural behavior of the wing, it was the logical first-step to conduct a static analysis. We applied the setup discussed in the previous section to the analysis.

Unfortunately, we did not get any useful results. Most of the time, the job would run for a while, eventually crashing

and raising “time increment too small” or “too many attempts made for this increment” error messages. Best case was when the simulation ran up to 20% of the time increments (refer to Fig. 15). However, that result isn’t usable because that means only 20% of the load was applied.

Fig. 15. Screenshot of last increment of the static analysis before crashing. This simulation failed at 20% time increment.

Looking into the warnings to help debug the issue, we noticed that the ”zero MOMENT everywhere” issue. We concluded that these errors were raised because we were using the membrane elements for the Mylar. Membrane elements have no bending stiffness; they behave like fabric or extremely thin sheets. However, even if we tried switching the element types to shell elements, we still ran into convergence issues.

2) Dynamic Explicit Analysis: Although using membrane elements led to issues regarding zero moments, a member of the teaching staff pointed out that they have always used membrane elements in dynamic analyses. This led us to conducting a dynamic explicit analysis. Although the dynamic explicit method is prone to inaccuracies, the solution always converges. Additionally, dynamic analyses can be configured to run a quasi-static analysis. Reconfiguring the loading and boundary conditions to run a quasi-static analysis, we were able to obtain results shown in Fig. 16.

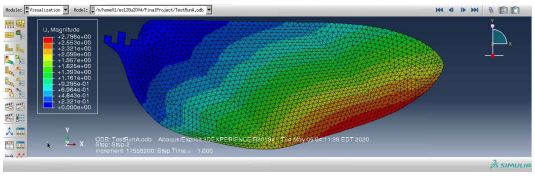

Fig. 16. Results obtained from the dynamic explicit analysis.

Unfortunately, these results proved to be unusable due to the oscillations present (refer to Fig. 17). A source of the oscillations comes from mass scaling [12]. In dynamic analysis, mass scaling is done in order to reduce computation time, which in our case was significant, about 4 hours per wing. However, it does have the effect of creating oscillations in the results. To counteract this, damping is added to the model through changing the bulk damping values in the STEP or material damping. Unfortunately, despite using mass scaling factors ranging from 50 to 1000 while adding a linear bulk viscosity damping factor ranging from 0.06 to 20 and adding material damping of $\alpha = \beta = 0.1$, this balancing act was unable to reduce the computation time and eliminate oscillations.

An alternative method to reduce oscillations proposed by a member of the teaching staff was to use a smooth step (refer to Figure 18 for a visual guide). Since the oscillations are caused

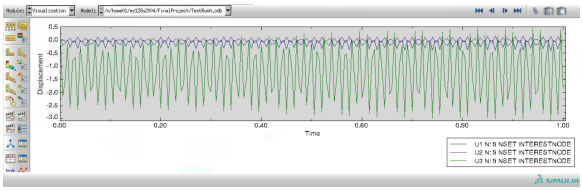

Fig. 17. Plot showing the displacement of a node along the leading edge. Due to the extreme oscillations, results were unusable.

by accelerations, minimizing the accelerations should reduce the oscillations. Unfortunately, there was not enough time to test this method out.

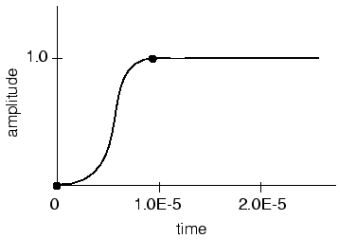

Fig. 18. Visual representation of a smooth step in ABAQUS. Image obtained from [13].

3) Dynamic Implicit Analysis: In an attempt to reduce the errors that occured in the explicit analysis, we switched over to using an implicit, quasi-static analysis. Compared to explicit, implicit is more accurate but does not guarantee convergence.

Unfortunately, the analysis did not yield any results at all. The program crashes when I was running the simulation locally, and on the cluster, the time steps were extremely small (Δt = 1.81E-13) that the simulation would not provide results in a reasonable amount of time.

Material redefinition was also looked at. For the Mylar, we thought that the errors in convergence could arise due to the potential nonlinear behavior. Using the Lame parameters [14], we were able to convert the linear elastic parameters to the Neo-Hookean coefficients (C10 = 624.46 MPa, D1 = 417.76E-06) [15]. Unfortunately, this also did not resolve the errors in the simulation.

IV. Conclusion and Future Work

Overall, this research experience has been amazing, one filled with learning and mastery. Through my work in the first half of the semester, I was able to gain a better understanding of the Robobee project and designing for smart-composite microstructures. This 2.5D manufacturing was completely new and challenged my current knowledge of design engineering. In the second half of the semester, despite the simulations not yielding usuable results, my understanding of finite-element methods is deeper and more comprehensive.

As hinted throughout the report, there is future work that can be done. Some of them are:

- Continue researching designs for multi-DOF robots to learn current methods of SCM design and apply it to the design of the vertical hopping robot.

- Test out new setups for the wing FEA. Currently, I'm thinking of testing out membrane pre-tensioning or utilizing tie-constraints with two separate sketches.

This research experience was my first one. Having been curious about what conducting research is like, this was a great opportunity to answer this curiosity. I hope to be able to continue the research process.

ACKNOWLEDGMENTS

I would like to thank Avik De (James S. McDonnell Foundation Postdoctoral Fellow) for his extensive mentorship and patience throughout the semester. Without him, the work done here would have not been possible.

I would also like to thank the course staff of ENG-128/228 (Prof. Katia Bertoldi, Connor McCann, Benjamin Gorrisen, and Mohamed Zanaty) for their extensive help and guidance for the finite element aspect of the project.

Finally, I would like to thank Oluwaseun Araromi, a postdoctral researcher in the Wood and Walsh lab and Eliot House tutor, for guiding me into the research process.

REFERENCES

[1] R. J. Wood, "The first takeoff of a biologically inspired at-scale robotic insect," *IEEE transactions on robotics*, vol. 24, no. 2, pp. 341–347, 2008.

[2] A. Calderón, Y. Chen, X. Yang, L. Chang, X.-T. Nguyen, E. Singer, and N. Pérez-Arancibia, "Control of flying robotic insects: A perspective and unifying approach," *arXiv preprint arXiv:1910.11911*, 2019.

[3] N. Doshi, B. Goldberg, R. Sahai, N. Jafferis, D. Aukes, R. J. Wood, and J. A. Paulson, "Model driven design for flexure-based microrobots," in *2015 IEEE/RSJ International Conference on Intelligent Robots and Systems (IROS)*. IEEE, 2015, pp. 4119–4126.

[4] J.-s. Koh, D. M. Aukes, B. Araki, S. Pohorecky, Y. Mulgaonkar, M. T. Tolley, V. Kumar, D. Rus, and R. J. Wood, *A Modular Folded Laminate Robot Capable of Multi Modal Locomotion*. Springer, p. 59–63. [Online]. Available: https://books.google.com/books?id=2pZtDgAAQBAJ&pg=PA60&lpg=PA60&dq=laminatemanufacturingofsphericaljoints&source=bl&ots=Wpo7_rqTE1&sig=ACfU3U0rlCzyaeVQQaFEW0K4utaNgXcKXw&hl=en&sa=X&ved=2ahUKEwjdx46_5oHoAhVCheAKHfNxCmgQ6AEwC3oECAYQAQ#v=onepage&q=laminatemanufacturingofsphericaljoints&f=false

[5] Y. Chen, K. Ma, and R. J. Wood, "Influence of wing morphological and inertial parameters on flapping flight performance," in *2016 IEEE/RSJ International Conference on Intelligent Robots and Systems (IROS)*. IEEE, 2016, pp. 2329–2336.

[6] N. T. Jafferis, E. F. Helbling, M. Karpelson, and R. J. Wood, "Untethered flight of an insect-sized flapping-wing microscale aerial vehicle," *Nature*, vol. 570, no. 7762, pp. 491–495, 2019.

[7] P. Chirarattananon, K. Y. Ma, and R. J. Wood, "Adaptive control of a millimeter-scale flapping-wing robot," *Bioinspiration & biomimetics*, vol. 9, no. 2, p. 025004, 2014.

[8] M. Smith, *ABAQUS/Standard User's Manual, Version 6.9*. United States: Dassault Systèmes Simulia Corp, 2009.

[9] D. T. Films, *Mylar® polyester film*. DuPont Teijin Films.

[10] N. Steel, *Pitch-Based Carbon Fiber with Low Modulus and High Heat Conduction*. Nippon Steel, 2001.

[11] J. P. Whitney and R. J. Wood, "Aeromechanics of passive rotation in flapping flight," *Journal of fluid mechanics*, vol. 660, pp. 197–220, 2010.

[12] G. Cocchetti, M. Pagani, and U. Perego, "Selective mass scaling for distorted solid-shell elements in explicit dynamics: optimal scaling factor and stable time step estimate," *International Journal for Numerical Methods in Engineering*, vol. 101, no. 9, pp. 700–731, 2015.

[13] "Smooth amplitude curves," https://abaqus-docs.mit.edu/2017/English/SIMACAEGSARefMap/simagsa-c-qsismoothampcve.htm.

[14] "Lamé parameters," Jan 2020. [Online]. Available: https://en.wikipedia.org/wiki/Lam_parameters

[15] "Hyperelastic behavior of rubberlike materials." [Online]. Available: https://classes.engineering.wustl.edu/2009/spring/mase5513/abaqus/docs/v6.6/books/usb/default.htm?startat=pt05ch17s05abm07.html#usb-mat-chyperelastic-neohooke